Translational Planar Cable-Direct-Driven Robots

Robert L. Williams II
Ohio University
Athens, Ohio

Paolo Gallina
University of Trieste
Trieste, Italy

Journal of Intelligent and Robotic Systems
Vol. 37, pp. 69-96
2003

Keywords: cable-direct-driven robots, actuation redundancy, statics workspace, dynamics, control, dynamic minimum torque estimation, translational tasks

Corresponding author:

Robert L. Williams II
Associate Professor
Department of Mechanical Engineering
257 Stocker Center
Ohio University
Athens, OH 45701-2979
Phone: (740) 593-1096
Fax: (740) 593-0476
E-mail: williar4@ohio.edu
URL: http://www.ent.ohiou.edu/~bobw

TRANSLATIONAL PLANAR CABLE-DIRECT-DRIVEN ROBOTS

Robert L. Williams II
Ohio University
Athens, OH

Paolo Gallina
University of Trieste
Trieste, ITALY

ABSTRACT

A planar cable-direct-driven robot (CDDR) architecture is introduced with only translational freedoms. The motivation behind this work is to improve the serious cable interference problem with existing CDDRs and to avoid configurations where negative cable tensions are required to exert general forces on the environment and during dynamic motions. These problems generally arise for rotational CDDR motions. Thus, we propose a class of purely translational CDDRs; of course, these are not general but may only perform tasks where no rotational motion or resistance of moments is required at the end-effector. This article includes kinematics and statics modeling, determination of the statics workspace (the space wherein all possible Cartesian forces may be exerted with only positive cable tensions), plus a dynamics model and simulated control for planar translational CDDRs. Examples are presented to demonstrate simulated control including feedback linearization of the 4-cable CDDR (with two degrees of actuation redundancy) performing a Cartesian task. We introduce an on-line dynamic minimum torque estimation algorithm to ensure all cable tensions remain positive for all motion; otherwise slack cables result from the CDDR dynamics and control is lost.

1. INTRODUCTION

Cable-direct-driven robots (CDDRs) are a type of parallel manipulator wherein the end-effector link is supported in-parallel by *n* cables with *n* tensioning motors. In addition to the well-known advantages of parallel robots relative to serial robots, CDDRs also have low mass and can have better stiffness than other parallel robots. Several CDDRs and cable-direct-driven haptic interfaces (CDDHIs) have been studied in the past, as now partially discussed. An early CDDR is the *Robocrane* developed by NIST (Albus et al., 1993) for use in shipping ports. This device is similar to an upside-down six-degrees-of-freedom (dof) Stewart platform, with six cables instead of hydraulic-cylinder legs. In this system, gravity is an implicit actuator that ensures cable tension is maintained at all times. Another CDDR is *Charlotte*, developed by McDonnell-Douglas (Campbell et al., 1995) for use on International Space Station. *Charlotte* is a rectangular box driven in-parallel by eight cables, with eight tensioning motors mounted on-board (one on each corner). Four CDDHIs have been built and tested, the *Texas 9-string*

(Lindemann and Tesar, 1989), the *SPIDAR* (Walairacht et al., 1999), the 7-cable master (Kawamura and Ito, 1993), and the 8-cable haptic interface (Williams, 1998). CDDRs and CDDHIs can be made lighter, stiffer, safer, and more economical than traditional serial robots and haptic interfaces since their primary structure consists of lightweight, high load-bearing cables. On the other hand, one major disadvantage is that cables can only exert tension and cannot push on the moving platform.

All of the devices discussed above are designed with actuation redundancy, i.e. more cables than wrench-exerting degrees-of-freedom (except for the *Robocrane*, where tensioning is provided by gravity) in attempt to avoid configurations where certain wrenches require an impossible compression force in one or more cables. Despite actuation redundancy, there exist subspaces in the potential workspace where some cables can lose tension; this problem generally is associated with rotational end-effector motion. This problem can be exacerbated by CDDR dynamics, hence the current article studies dynamics and control of planar translational CDDRs, with no rotational motion allowed. Roberts et al. (1998) developed an algorithm for CDDRs to predict if all cables are under tension in a given configuration while supporting the robot weight only. These authors also present the inverse kinematics and fault tolerance of Charlotte-type (Campbell et al., 1995) CDDRs, but no dynamics modeling is presented. The authors have presented CDDHI design (with translational and rotational motion) with regard to exerting all possible wrenches with only positive cable tensions and with regard to avoiding cable interference (Williams and Gallina, 2002). In that work it was found that cable interference dominates.

Recently there has been a lot of work concerning CDDR-related research. Choe et al. (1996) point out that wire-driven robots must provide stiffness in all six Cartesian directions, even if the desired motion is in a subspace of general Cartesian motion. The current article handles this issue by assuming that our planar end-effector is supported by a base plate for stiffness perpendicular to the plane, and by not requiring moment resistance by the end-effector. Though not directly related to CDDRs, Kock and Schumacher (2000) present a discussion of actuation redundancy for more conventional parallel manipulators. Barrette and Gosselin (2000) present a systematic kinematic and workspace analysis of planar CDDRs with translational and rotational motion.

Most proposed CDDRs and CDDHIs involve both translational and rotational motion of the end-effector link guided by cables. (An exception is the *SPIDAR* (Walairacht et al., 1999), which is a spatial 4-cable haptic interface reading translations only and providing three Cartesian forces to the human finger.) All CDDRs and CDDHIs with translational and rotational motion suffer from the potential of cable interference and reduced statics workspaces wherein some negative cable tensions would be required, which is infeasible. The basic idea behind this article is to introduce a CDDR with only translational motion that can be used for a reduced set of tasks: axisymmetric tasks that require no rotational motions or moment resistance by the end-effector. Example tasks include planar spray painting, spot and seam welding, limited planar assembly tasks, and translational/force-only haptic interface. The main objective of this work is to benefit from potential advantages of CDDRs without the cable interference and negative cable tension problems; an obvious drawback is the limited range of tasks.

This article describes two candidate translational planar CDDRs, presents kinematics modeling, followed by statics modeling, a method for attempting to maintain positive cable tensions, and a method for determining the statics workspace, wherein all possible Cartesian forces may be exerted, with only positive cable tensions. The article then presents dynamics modeling (resulting in a nonlinear, coupled dynamics model), followed by Cartesian trajectory control simulation employing Cartesian PD control and feedback linearization for planar CDDRs with one and two degrees of actuation redundancy. An on-line dynamic minimum torque estimation algorithm is developed to avoid slack cables due to dynamics. Examples are then presented for the dynamics model and simulated control, for the translational planar 4-cable CDDR with two degrees of actuation redundancy.

2. CABLE-DIRECT-DRIVEN ROBOTS (CDDRs)

In this article a translational planar CDDR consists of a single end-effector point driven in parallel by *n* cables controlled by *n* tensioning actuators. Since no rotational motions and no moment resistance are required at the end-effector, all *n* cables meet in a single point, and the end-effector is modeled as a point mass. Figures 1 and 2 show the translational planar 3-cable and 4-cable CDDR kinematics diagrams. We assume that a base plate supports the end-effector in the *XY* plane so no *Z* stiffness need be provided by the planar CDDR, which is impossible. Also, we assume no end-effector moment resistance is required by the subset of planar translational tasks in this article; no rotational motions or *Z* moment resistance is possible with the CDDRs of Figs. 1 and 2.

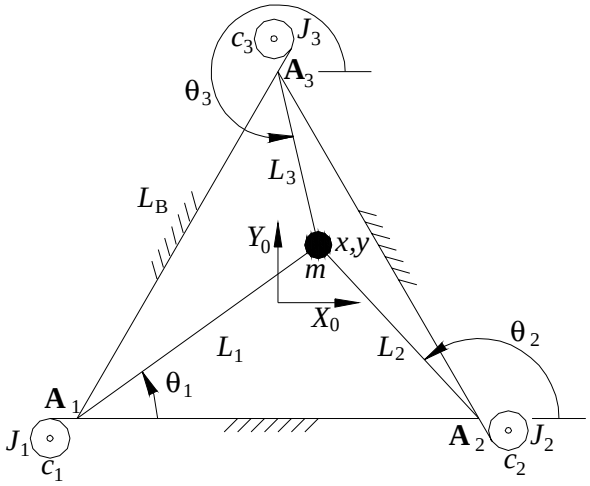

Figure 1. Planar 3-Cable CDDR Diagram

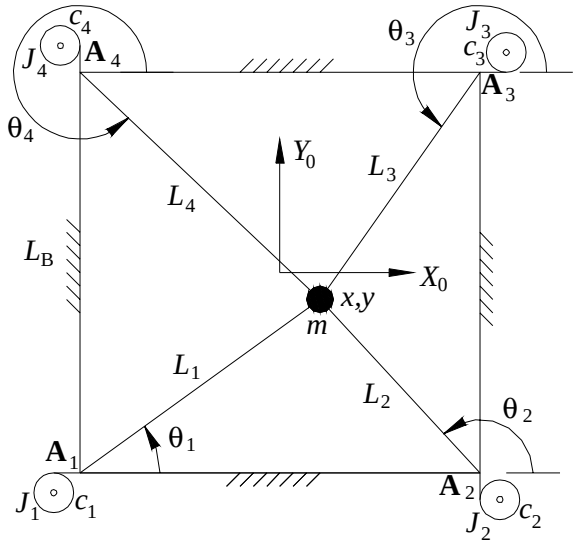

Figure 2. Planar 4-Cable CDDR Diagram

For 2-dof planar translations there must be at least two cables. Since cables can only exert tension on the end-effector, there must be more cables to avoid configurations where the CDDR cables can be slack and lose control. Figure 1 represents one degree of actuation redundancy, i.e. three cables to achieve the two Cartesian degrees-of-freedom $\mathbf{X} = \{x \quad y\}^T$; the CDDR in Fig. 2 has two degrees of actuation redundancy. These scenarios

represent actuation redundancy but not kinematic redundancy. That is, there is an extra motor or motors which provide infinite choices for applying 2-dof Cartesian force vectors, but the moving point has only two Cartesian degrees-of-freedom ($\mathbf{X} = \{x \quad y\}^T$, the components of the position vector from the origin of $\{\mathbf{0}\}$ to the moving point, expressed in $\{\mathbf{0}\}$ coordinates).

Figures 1 and 2 show the inertially-fixed reference frame $\{\mathbf{0}\}$ whose origin is the centroid of the base polygon; the regular base polygon (triangle and square, respectively) has sides of fixed length L_B; each cable is passed through the ground link at the fixed points $\mathbf{A}_i = \{A_{ix} \quad A_{iy}\}^T$; the length of each cable is denoted as L_i, and the cable angles are θ_i ($i = 1, \cdots, n$). The end-effector point mass is *m* and the lumped motor shaft/cable pulley rotational inertias for each actuator are J_i ($i = 1, \cdots, n$). We also include viscous damping coefficients c_i ($i = 1, \cdots, n$) at each motor shaft to provide a linear model for the system friction. The cable pulley radius for each actuator is r_i ($i = 1, \cdots, n$; not shown in Figs. 1 or 2).

Theoretically the moving point can reach any point within the base polygon, if cable lengths can go to zero. Also, the potential for cable/cable and cable/end-point interference is non-existent for the CDDR designs of Figs. 1 and 2. The potential certainly exists for interference between cables and workspace items and/or humans, but this problem can be minimized by design in the case of planar CDDRs.

3. CDDR KINEMATICS MODELING

This section presents the inverse and forward translational position and velocity kinematics analysis for planar CDDRs. Inverse kinematics is required for control, and forward kinematics is required for simulation and sensor-based control. Kinematics is concerned with relating the active joint variables and rates to the Cartesian position and rate variables of the moving point. The cable angles and rates are also involved. Assuming all cables always remain in tension, CDDR kinematics is similar to in-parallel-actuated robot kinematics (e.g. Tsai (1999); Gosselin (1996)); however, with CDDRs the joint space is overconstrained with respect to the Cartesian space. Again, in this article we only consider translational motion and forces, associated with a reduced set of possible planar tasks.

3.1 Position Kinematics

The inverse position kinematics problem is stated: given the Cartesian position $\mathbf{X} = \{x \quad y\}^T$ calculate the cable lengths L_i. The solution is simply calculating the Euclidean norm between the moving point $\mathbf{X} = \{x \quad y\}^T$ and each fixed ground link vertex $\mathbf{A}_i$:

$$L_i = \sqrt{(x - A_{ix})^2 + (y - A_{iy})^2} \qquad i = 1, \cdots, n \tag{1}$$

For use in velocity kinematics and statics, we require the cable angles:

$$\theta_i = \tan^{-1}\left(\frac{y - A_{iy}}{x - A_{ix}}\right) \qquad i = 1, \cdots, n \tag{2}$$

The quadrant-specific inverse tangent function must be used in (2).

The forward position kinematics problem is stated: given the cable lengths L_i, calculate the Cartesian position $\mathbf{X} = \{x \quad y\}^T$. This problem is overconstrained and assumes a consistent input of L_i. First we consider cables 1 and 2. This problem can be simplified by shifting a new reference frame origin to $\mathbf{A}_1$ whose *XY* directions are identical to $\{\mathbf{0}\}$; in this new frame $\mathbf{A}_1 = \{0 \quad 0\}^T$ and $\mathbf{A}_2 = \{L_B \quad 0\}^T$. Then the solution to the forward position kinematics problem is the intersection of two circles, one centered at $\mathbf{A}_1$ with radius L_1 and the second centered at $\mathbf{A}_2$ with radius L_2; the solution is:

$$x = \frac{L_B^2 + L_1^2 - L_2^2}{2L_B} \qquad y = \pm\sqrt{L_1^2 - x^2} \tag{3}$$

We choose the positive solution for *y* in (3) to ensure the forward position kinematics solution lies within the ground polygon. Therefore, from the multiple possibilities (we could have used any two cables to obtain the solution), there is a unique correct solution. Note the value of *x* in (3) is unique due to the special geometry for cables 1 and 2 (both *y* values have the same *x* value). To finish, this solution (3) must be shifted back to the $\{\mathbf{0}\}$ frame reference. This solution applies to any planar *n*-cable CDDR with a point end-effector.

After employing (3) for the forward position kinematics solution, it is a good idea to use the inverse position kinematics solution (1) for all remaining cables ($i = 3, \cdots, n$) to verify that the L_i input was consistent.

3.2 Velocity Kinematics

To derive the velocity kinematics equations we consider the i^{th} cable vector-loop-closure equation $\{x \quad y\}^T = \{A_{ix} + L_i c\theta_i \quad A_{iy} + L_i s\theta_i\}^T$, where $c\theta_i = \cos\theta_i$ and $s\theta_i = \sin\theta_i$. The time derivative yields:

$$\begin{Bmatrix} \dot{x} \\ \dot{y} \end{Bmatrix} = \begin{bmatrix} c\theta_i & -L_i s\theta_i \\ s\theta_i & L_i c\theta_i \end{bmatrix} \begin{Bmatrix} \dot{L}_i \\ \dot{\theta}_i \end{Bmatrix} \qquad i = 1, \cdots, n \tag{4}$$

We invert this i^{th} cable Jacobian matrix to yield:

$$\begin{Bmatrix} \dot{L}_i \\ \dot{\theta}_i \end{Bmatrix} = \begin{bmatrix} c\theta_i & s\theta_i \\ -s\theta_i / L_i & c\theta_i / L_i \end{bmatrix} \begin{Bmatrix} \dot{x} \\ \dot{y} \end{Bmatrix} \qquad i = 1, \cdots, n \tag{5}$$

Since we are interested in relating active cable length rates to the Cartesian rates, we can extract the first row of (5) to construct the overall CDDR inverse velocity solution. For the 3- and 4-cable cases:

$$\begin{Bmatrix} \dot{L}_1 \\ \dot{L}_2 \\ \dot{L}_3 \end{Bmatrix} = \begin{bmatrix} c\theta_1 & s\theta_1 \\ c\theta_2 & s\theta_2 \\ c\theta_3 & s\theta_3 \end{bmatrix} \begin{Bmatrix} \dot{x} \\ \dot{y} \end{Bmatrix} \qquad \begin{Bmatrix} \dot{L}_1 \\ \dot{L}_2 \\ \dot{L}_3 \\ \dot{L}_4 \end{Bmatrix} = \begin{bmatrix} c\theta_1 & s\theta_1 \\ c\theta_2 & s\theta_2 \\ c\theta_3 & s\theta_3 \\ c\theta_4 & s\theta_4 \end{bmatrix} \begin{Bmatrix} \dot{x} \\ \dot{y} \end{Bmatrix} \tag{6}$$

Note that though we eliminated $\dot{\theta}_i$ from the velocity equations, cable angles θ_i from (2) are required in (6). The general form of (6) is $\dot{\mathbf{L}} = \mathbf{M}\dot{\mathbf{X}}$ where $\dot{\mathbf{L}}$ is the vector of *n* cable rates, $\mathbf{M}$ is the translational CDDR inverse Jacobian matrix, and $\dot{\mathbf{X}} = \{\dot{x} \quad \dot{y}\}^T$ is the Cartesian velocity vector for the moving point, shared by all *n* cables. Considering the inverse velocity problem of conventional serial robots, the result (6) is amazing: the inverse velocity problem is solved directly (the inversion was handled symbolically from (4) to (5)) with little computation and there is no singularity problem.

However, to solve the forward velocity kinematics problem we must invert the form of (6): $\dot{\mathbf{X}} = \mathbf{M}^{-1}\dot{\mathbf{L}}$. Due to redundant actuation, $\mathbf{M}$ is not square but is of dimension *n*x2 for the planar case; therefore we cannot invert $\mathbf{M}$ but we have two choices for the forward velocity solution: 1) choose only two cables to make a reduced, square, inverse Jacobian matrix. For instance, as in the forward position kinematics solution, choose cables 1 and 2. The forward velocity solution for the 3-cable CDDR is then $\dot{\mathbf{X}} = \mathbf{M}_{12}{}^{-1}\dot{\mathbf{L}}_{12}$ where $\mathbf{M}_{12}$ is $\mathbf{M}$ with row 3 removed and $\dot{\mathbf{L}}_{12}$ is the vector containing the first two cable rates. This approach can readily be extended to the 4-cable CDDR. After forward velocity solution, ensure that the $\dot{\mathbf{L}}$ inputs were consistent by evaluating the neglected row(s) of (6). 2) The alternate forward velocity solution approach, assuming consistent $\dot{\mathbf{L}}$ inputs, is to use the left pseudoinverse: $\dot{\mathbf{X}} = \mathbf{M}^{\#}\dot{\mathbf{L}}$, where $\mathbf{M}^{\#} = \left(\mathbf{M}^{\mathbf{T}}\mathbf{M}\right)^{-1}\mathbf{M}^{\mathbf{T}}$. The second alternate solution approach may be preferable in hardware application since any errors in $\dot{\mathbf{L}}$ measurements will be somewhat mitigated by the pseudoinverse, compared to using only two components of $\dot{\mathbf{L}}$.

Via either solution approach, the forward velocity solution is subject to singularities. The singularity conditions are derived from the determinants of the three possible 2x2 square submatrices of $\mathbf{M}$:

$$\begin{aligned} \sin(\theta_2 - \theta_1) &= 0 & \theta_2 - \theta_1 &= 0, \pi, \cdots \\ \sin(\theta_3 - \theta_2) &= 0 & \theta_3 - \theta_2 &= 0, \pi, \cdots \\ \sin(\theta_1 - \theta_3) &= 0 & \theta_1 - \theta_3 &= 0, \pi, \cdots \end{aligned} \tag{7}$$

The singularities only occur when two cables lie along a straight line; this is only possible at the edges of the theoretical kinematic workspace, i.e. along the edges of the ground polygon. Equation (7) gives the 3-cable CDDR singularities. The 4-cable CDDR singularities are similar (i.e. only along the edges of the ground square).

4. CDDR STATICS MODELING

In this article, the workspace wherein all cables are under positive tension while exerting all possible Cartesian forces is called the statics workspace. Statics modeling and attempting to maintain positive cable tension are presented in this section. We use a simple method to determine the extent of the statics workspace, i.e. the workspace wherein all possible forces can be applied with positive cable tensions.

4.1 Statics Modeling

This section presents statics modeling for translational planar CDDRs. For static equilibrium the sum of forces exerted on the moving point by the cables must equal the resultant external force exerted on the environment. Figure 3 shows the statics free-body diagram for the planar 4-cable CDDR. The statics equations are:

$$\sum_{i=1}^{n} \mathbf{t}_i = -\sum_{i=1}^{n} t_i \hat{\mathbf{L}}_i = \mathbf{F}_R \tag{8}$$

In this article gravity is ignored because it is assumed to be perpendicular to the CDDR plane; we assume the moving end-effector point is supported on a base plate. All vectors are expressed in $\{\mathbf{0}\}$ (see Figs. 1 and 2). In (8), t_i is the cable tension applied to the i^{th} cable (opposite the cable length unit direction $\hat{\mathbf{L}}_i = \{c\theta_i \quad s\theta_i\}^T$ because vector $\mathbf{t}_i$ must be in tension). $\mathbf{F}_R = \{f_x \quad f_y\}^T$ is the resultant vector force exerted on the environment by the moving point. Substituting terms into (8) yields the form $\mathbf{ST} = \mathbf{F}_R$, where $\mathbf{S} = \left[-\hat{\mathbf{L}}_1 \quad \cdots \quad -\hat{\mathbf{L}}_n\right]$ is the 2xn translational Statics Jacobian matrix and $\mathbf{T} = \{t_1 \quad \cdots \quad t_n\}^T$ is the vector of scalar cable tensions t_i. For the 3- and 4-cable CDDRs:

$$\begin{bmatrix} -c\theta_1 & -c\theta_2 & -c\theta_3 \\ -s\theta_1 & -s\theta_2 & -s\theta_3 \end{bmatrix} \begin{Bmatrix} t_1 \\ t_2 \\ t_3 \end{Bmatrix} = \begin{Bmatrix} f_x \\ f_y \end{Bmatrix} \qquad \begin{bmatrix} -c\theta_1 & -c\theta_2 & -c\theta_3 & -c\theta_4 \\ -s\theta_1 & -s\theta_2 & -s\theta_3 & -s\theta_4 \end{bmatrix} \begin{Bmatrix} t_1 \\ t_2 \\ t_3 \\ t_4 \end{Bmatrix} = \begin{Bmatrix} f_x \\ f_y \end{Bmatrix} \tag{9}$$

Note that there is a special duality between force and inverse velocity: these respective Jacobian matrices are related by $\mathbf{S} = -\mathbf{M}^T$; compare (6) and (9). The statics equations (9) can be inverted in an attempt to exert general Cartesian forces while maintaining positive cable tension. This is presented in the next subsection.

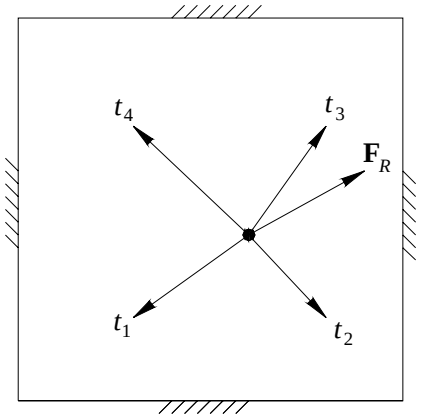

Figure 3. Planar 4-Cable CDDR Statics Diagram

4.2 Maintaining Positive Cable Tension

For CDDRs with actuation redundancy, (9) is underconstrained which means that there are infinite solutions to the cable tension vector $\mathbf{T}$ to exert the given Cartesian force $\mathbf{F}_R$. To invert (9) (solving for the required cable tensions $\mathbf{T}$ given the desired force $\mathbf{F}_R$) we adapt the well-known particular and homogeneous solution from rate control of kinematically-redundant serial manipulators:

$$\mathbf{T} = \mathbf{S}^{+}\mathbf{F}_R + \left(\mathbf{I}_n - \mathbf{S}^{+}\mathbf{S}\right)\mathbf{z} \tag{10}$$

where $\mathbf{I}_n$ is the *n*x*n* identity matrix, **z** is an arbitrary *n*-vector, and $\mathbf{S}^{+} = \mathbf{S}^T\left(\mathbf{S}\mathbf{S}^T\right)^{-1}$ is the *n*x2 underconstrained Moore-Penrose pseudoinverse of **S**. The first term of (10) is the particular solution to achieve the desired force, and the second term is the homogeneous solution that maps **z** to the null space of **S**.

4.2.1 One Degree of Actuation Redundancy. For CDDRs with only one degree of actuation redundancy (the planar 3-cable case in this article), the positive cable tension method of Shen et al. (1994) is adapted to determine the extent of the statics workspace. For actuation redundancy of degree one, an equivalent expression for (10) is:

$$\mathbf{T} = \begin{Bmatrix} t_{P1} \\ t_{P2} \\ t_{P3} \end{Bmatrix} + a\begin{Bmatrix} n_1 \\ n_2 \\ n_3 \end{Bmatrix} \tag{11}$$

where the particular solution $\mathbf{S}^{+}\mathbf{F}_R$ is the first term in (11) and the homogeneous solution is expressed as the kernel vector of **S** ($\mathbf{N} = \{n_1 \quad n_2 \quad n_3\}^T$) multiplied by arbitrary scalar *a*.

The method we adapt from Shen et al. (1994) to determine if a given point lies within the statics workspace for a given CDDR is simple. To ensure positive tensions t_i on all cables *i* = 1,2,3, *for all possible exerted forces*, it is necessary and sufficient that all kernel vector components (n_i, *i* = 1,2,3) have the same sign. That is, for a given point to lie within the statics workspace, all $n_i > 0$ OR all $n_i < 0$ (*i* = 1,2,3). If one of these two conditions

is satisfied, regardless of the particular solution, we can find a scalar *a* in (11) which guarantees that all cable tensions **T** are positive by adding (or subtracting) enough homogeneous solution. Note a strict inequality is required; if one or more $n_i = 0$, the point in question does not lie within the statics workspace. This method is simple but powerful since we needn't consider specific forces, but it works for *all possible forces*. It should also be noted that while we demonstrate this method for the translational planar 3-cable CDDR, it is applicable to any planar and spatial CDDR with one degree of actuation redundancy.

The method to calculate each kernel vector component is $n_i = (-1)^{i+1}|\mathbf{S}_i|$, where $|\mathbf{S}_i|$ is the determinant of the 2x2 submatrix of **S** with column *i* removed. Applying this to the 3-cable CDDR yields:

$$\mathbf{N} = \begin{Bmatrix} n_1 \\ n_2 \\ n_3 \end{Bmatrix} = \begin{Bmatrix} \sin(\theta_3 - \theta_2) \\ \sin(\theta_1 - \theta_3) \\ \sin(\theta_2 - \theta_1) \end{Bmatrix} \tag{12}$$

Now, the allowable cable angle ranges are $0 \le \theta_1 \le 60^\circ$, $120^\circ \le \theta_2 \le 180^\circ$, and $240^\circ \le \theta_3 \le 300^\circ$. Therefore, the three possible delta angle ranges in (12) are $60^\circ \le \theta_3 - \theta_2 \le 180^\circ$, $-300^\circ \le \theta_1 - \theta_3 \le -180^\circ$, and $60^\circ \le \theta_2 - \theta_1 \le 180^\circ$. Note all three ranges are identical since the second condition is identical to $60^\circ \le \theta_1 - \theta_3 \le 180^\circ$. The *sine* of all these delta angles is always positive as long as $60^\circ \le \theta_j - \theta_k < 180^\circ$ (the *sine* is zero when any delta angle is equal to 180°). Therefore, *the entire allowable kinematic workspace of the base triangle is also the statics workspace*! So, there is no limitation due to considering only positive cable tensions! On the edge of the base triangle one $n_i = 0$ and thus the triangle edges are not in the statics workspace. Recall from the forward velocity solution presented in Section 3.2, the triangle edges also correspond to kinematic singularities. At all points outside of the base triangle, 2 components of the kernel vector **N** have the same sign and the other component has the opposite sign so outside the base triangle is also outside of the statics workspace.

For on-line pseudostatic control of a planar CDDR with one degree of actuation redundancy, the cable tensions for control are calculated by (11) and (12), choosing *a* so that one component of **T** is zero (or, in practical application, a small positive value) and the remaining terms are positive.

4.2.2 Two Degrees of Actuation Redundancy. For CDDRs with two or more degrees of actuation redundancy (the planar 4-cable case in this article), determination of the statics workspace and the method for maintaining positive cable tensions are more complicated. For actuation redundancy of degree two, an equivalent expression for (10) is:

$$\mathbf{T} = \begin{Bmatrix} t_{P1} \\ t_{P2} \\ t_{P3} \\ t_{P4} \end{Bmatrix} + a \begin{Bmatrix} n_1 \\ n_2 \\ n_3 \\ n_4 \end{Bmatrix} + b \begin{Bmatrix} p_1 \\ p_2 \\ p_3 \\ p_4 \end{Bmatrix} \tag{13}$$

where the particular solution $\mathbf{S}^{+}\mathbf{F}_R$ is again the first term in (13) and the homogeneous solution is expressed as the two kernel vectors of $\mathbf{S}$ ($\mathbf{N} = \{n_1 \quad n_2 \quad n_3 \quad n_4\}^T$ and $\mathbf{P} = \{p_1 \quad p_2 \quad p_3 \quad p_4\}^T$) multiplied by arbitrary scalars *a* and *b*. Given (13), the condition for a CDDR configuration to lie within the statics workspace is:

$$a \begin{Bmatrix} n_1 \\ n_2 \\ n_3 \\ n_4 \end{Bmatrix} + b \begin{Bmatrix} p_1 \\ p_2 \\ p_3 \\ p_4 \end{Bmatrix} > \begin{Bmatrix} 0 \\ 0 \\ 0 \\ 0 \end{Bmatrix} \tag{14}$$

Divide the workspace into four sectors as in Fig. 4. We can construct a different null space basis for each sector. This is required to demonstrate that the entire workspace is within the statics workspace.

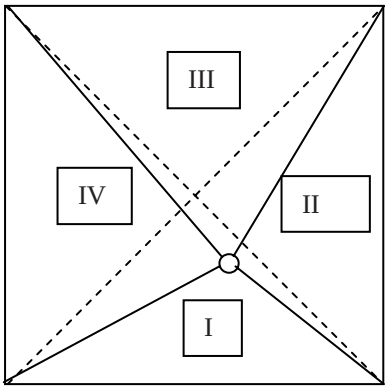

Figure 4. Planar 4-Cable CDDR Workspace Sectors

Case I: Let us suppose that the end-effector point is in the first sector. A possible basis for the null space is:

$$\mathbf{N} = \begin{Bmatrix} \sin(\theta_4 - \theta_2) \big/ \sin(\theta_2 - \theta_1) \\ \sin(\theta_1 - \theta_4) \big/ \sin(\theta_2 - \theta_1) \\ 0 \\ 1 \end{Bmatrix} \qquad \mathbf{P} = \begin{Bmatrix} \sin(\theta_3 - \theta_2) \big/ \sin(\theta_2 - \theta_1) \\ \sin(\theta_1 - \theta_3) \big/ \sin(\theta_2 - \theta_1) \\ 1 \\ 0 \end{Bmatrix} \tag{15}$$

If the end-effector lies within sector I, the allowable cable angle ranges are $0° < \theta_1 \le 45°$, $135° \le \theta_2 < 180°$, $225° \le \theta_3 < 270°$, and $270° < \theta_4 \le 315°$. Note that the sector triangle edges are included. The possible delta angle ranges are $90° < \theta_4 - \theta_2 < 135°$, $90° < \theta_2 - \theta_1 < 180°$, $-270° < \theta_1 - \theta_3 < -180°$, $-315° < \theta_1 - \theta_4 < -225°$, and

$45° < \theta_3 - \theta_2 < 135°$. Therefore all the sine functions in (15) are positive or null and any combination of **N** and **P** (with positive coefficients *a* and *b*) always has positive components as required in (14). In conclusion, the first sector belongs to the statics workspace.

Case II: Let us suppose that the end-effector point is in the second sector. We can choose a different basis for the null space:

$$\mathbf{N} = \begin{Bmatrix} 0 \\ \sin(\theta_4 - \theta_3) / \sin(\theta_3 - \theta_2) \\ \sin(\theta_2 - \theta_4) / \sin(\theta_3 - \theta_2) \\ 1 \end{Bmatrix} \qquad \mathbf{P} = \begin{Bmatrix} 1 \\ \sin(\theta_1 - \theta_3) / \sin(\theta_3 - \theta_2) \\ \sin(\theta_2 - \theta_1) / \sin(\theta_3 - \theta_2) \\ 0 \end{Bmatrix} \tag{16}$$

If the end-effector lies within sector II, the allowable cable angle ranges are $0° < \theta_1 \le 45°$, $90° < \theta_2 \le 135°$, $225° \le \theta_3 < 270°$, and $315° \le \theta_4 < 360°$. The possible delta angle ranges are $45° < \theta_4 - \theta_3 < 135°$, $-225° < \theta_2 - \theta_4 < -180°$, $-270° < \theta_1 - \theta_3 < -180°$, $45° < \theta_2 - \theta_1 < 135°$, and $90° < \theta_3 - \theta_2 < 180°$. Therefore, all sine functions in (16) are positive or null and any combination of **N** and **P** (with positive coefficients *a* and *b*) always has positive components. In conclusion, the second sector also belongs to the statics workspace.

The last two cases are similar. Choose:

$$\mathbf{N} = \begin{Bmatrix} 0 \\ 1 \\ \sin(\theta_2 - \theta_4) / \sin(\theta_4 - \theta_3) \\ \sin(\theta_3 - \theta_2) / \sin(\theta_4 - \theta_3) \end{Bmatrix} \qquad \mathbf{P} = \begin{Bmatrix} 1 \\ 0 \\ \sin(\theta_1 - \theta_4) / \sin(\theta_4 - \theta_3) \\ \sin(\theta_3 - \theta_1) / \sin(\theta_4 - \theta_3) \end{Bmatrix} \tag{17}$$

as a suitable basis for sector III and:

$$\mathbf{N} = \begin{Bmatrix} \sin(\theta_3 - \theta_4) / \sin(\theta_4 - \theta_1) \\ 0 \\ 1 \\ \sin(\theta_1 - \theta_3) / \sin(\theta_4 - \theta_1) \end{Bmatrix} \qquad \mathbf{P} = \begin{Bmatrix} \sin(\theta_2 - \theta_4) / \sin(\theta_4 - \theta_1) \\ 1 \\ 0 \\ \sin(\theta_1 - \theta_2) / \sin(\theta_4 - \theta_1) \end{Bmatrix} \tag{18}$$

as a suitable basis for sector IV. The conclusion for each case is identical, i.e. the third and fourth sectors also belong to the statics workspace, including all internal triangle edges. The only point we did not take into account is the center of the square, but in this case the basis of the null space consists of only one vector $\mathbf{N} = \{1 \quad 1 \quad 1 \quad 1\}^T$ because the rank of **S** degenerates to one. Clearly this special case is within the statics workspace since it easily satisfies (14).

Therefore, we have shown that *the entire allowable kinematic workspace of the base square is also the statics workspace*! The edge of the base square (which correspond to kinematic singularities) and all points outside

of the base square are outside of the statics workspace. This result makes sense given the 3-cable results since the addition of another cable can only help the statics workspace.

In Section 6.2 we will present a general method for on-line control of a planar CDDR with two (or more) degrees of actuation redundancy (i.e. find optimal *a* and *b* for (13)). We will do this with regard to dynamics; since the pseudostatic condition is a limiting subset of the general dynamics case, we now move on to dynamics modeling.

5. CDDR DYNAMICS MODELING

This section presents dynamics modeling for translational planar CDDRs. The translational planar 3- and 4-cable CDDRs are shown in Figs. 1 and 2. Dynamics modeling is required for improved control (compared to using kinematics and statics modeling only) when CDDRs are to provide high velocities and accelerations in translational motion. Dynamics modeling is concerned with relating the Cartesian translational motion of the moving CDDR end-effector point to the required active joint torques. Due to the cable actuation, CDDR dynamics modeling is not very similar to in-parallel-actuated robot dynamics modeling (e.g. Tsai (1999); Gosselin (1996)). Another complicating factor is that the joint space is overconstrained with respect to the Cartesian space due to redundant actuation.

For the dynamics model derived in this section we assume that the CDDR cables are massless and perfectly stiff so we do not consider their inertias or spring stiffnesses. We further ignore the Coulomb friction and instead model linear viscous friction to account for the frictional losses. Despite these simplifications, the resulting model is coupled and nonlinear. We now present the Cartesian, actuator, and overall system dynamics models.

5.1 Cartesian Dynamics Model

The free-body diagram for the moving end-effector point is simple and hence not shown. The 2-*dof* Cartesian dynamic model for the end-effector is given by:

$$\mathbf{m}\ddot{\mathbf{X}} = \mathbf{F} \tag{19}$$

where the Cartesian mass matrix is $\mathbf{m} = \begin{bmatrix} m & 0 \\ 0 & m \end{bmatrix}$, $\mathbf{X} = \{x \quad y\}^T$ is the end-effector position and $\mathbf{F}$ is the resultant of all *n* cable forces (tensions) acting on the end-effector.

5.2 Actuator Dynamics Model

We also take into consideration the dynamic behavior of the lumped motor shaft/cable pulley; the free-body diagram for the i^{th} motor shaft/cable pulley subsystem is shown in Fig. 5.

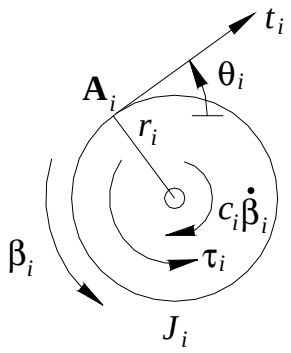

Figure 5. Free-Body Diagram for the i^{th} Pulley/Shaft

The combined motor shaft/cable pulley dynamics equations are expressed by the relationship:

$$\mathbf{J}\ddot{\boldsymbol{\beta}} + \mathbf{C}\dot{\boldsymbol{\beta}} = \boldsymbol{\tau} - r\mathbf{T} \tag{20}$$

where: $\mathbf{J} = \begin{bmatrix} J_1 & & 0 \\ & \ddots & \\ 0 & & J_n \end{bmatrix}$ and $\mathbf{C} = \begin{bmatrix} c_1 & & 0 \\ & \ddots & \\ 0 & & c_n \end{bmatrix}$

are diagonal matrices with rotational inertia and rotational viscous damping coefficients on the diagonal, all cable pulley radii (r_i in Fig. 5) are identical ($r_i = r$; $i = 1, \cdots, n$), $\boldsymbol{\tau} \in R^n$ is the vector of torques exerted by the motors, $\mathbf{T} \in R^n$ is the vector of cable tensions t_i, and $\boldsymbol{\beta} \in R^n$ is the vector of pulley angles. Since the cables can only exert positive tensions (they cannot push), to express the cable tensions as a function of the motor torques and angular motion from (20), we obtain:

$$\mathbf{T} = pos\left(\frac{1}{r}\left(\boldsymbol{\tau} - \mathbf{J}\ddot{\boldsymbol{\beta}} - \mathbf{C}\dot{\boldsymbol{\beta}}\right)\right) \tag{21}$$

where the symbol $pos()$ means we take the value of each vector component that is positive and we set to zero those components that were originally negative. Let us suppose that the torque on each motor is large enough to make all cables remain in tension at all times. Under this assumption:

$$\mathbf{T} = \frac{1}{r}\left(\boldsymbol{\tau} - \mathbf{J}\ddot{\boldsymbol{\beta}} - \mathbf{C}\dot{\boldsymbol{\beta}}\right) \tag{22}$$

5.3 System Dynamics Model

We now derive the overall system dynamics model by combining the Cartesian and actuator dynamics equations of motion. The statics relationship $\mathbf{S}\mathbf{T} = \mathbf{F}_R$ between cable tensions and end-effector forces was derived in Section 4.1, where the 2x*n* statics Jacobian matrices **S** for the 3-and 4-cable CDDRs were given in (9); the form is:

$$\mathbf{S} = \begin{bmatrix} -\cos\theta_1 & \cdots & -\cos\theta_n \\ -\sin\theta_1 & \cdots & -\sin\theta_n \end{bmatrix} \tag{23}$$

where θ_i ($i = 1, \cdots, n$) are the cable angles (see Figs. 1 and 2).

We now need an inverse kinematics mapping relating the pulley angles β_i ($i = 1, \cdots, n$) expressed as functions of the end-effector position $\mathbf{X} = \{x \quad y\}^T$. Let us define all β_i to be zero when the end-effector is located at the origin of frame $\{\mathbf{0}\}$. From this position, a right-handed positive angle β_i on one pulley will cause a negative change ΔL_i in cable length i: $\beta_i r = -\Delta L_i$. The change in cable length i is $\Delta L_i = L_i - L_{0i}$ where $L_i = \sqrt{(x - A_{ix})^2 + (y - A_{iy})^2}$ is the general length for cable i from the inverse position solution given in (1) and $L_{0i} = \sqrt{(A_{ix})^2 + (A_{iy})^2}$ is the initial length for cable i. Therefore:

$$\boldsymbol{\beta} = \begin{Bmatrix} \beta_1(\mathbf{X}) \\ \vdots \\ \beta_n(\mathbf{X}) \end{Bmatrix} = \frac{1}{r} \begin{Bmatrix} L_{01} - \sqrt{(x - A_{1x})^2 + (y - A_{1y})^2} \\ \vdots \\ L_{0n} - \sqrt{(x - A_{nx})^2 + (y - A_{ny})^2} \end{Bmatrix} \tag{24}$$

Successive time derivatives of (24) yield:

$$\begin{aligned} \dot{\boldsymbol{\beta}} &= \frac{\partial \boldsymbol{\beta}}{\partial \mathbf{X}} \dot{\mathbf{X}} \\ \ddot{\boldsymbol{\beta}} &= \frac{d}{dt}\left(\frac{\partial \boldsymbol{\beta}}{\partial \mathbf{X}}\right)\dot{\mathbf{X}} + \frac{\partial \boldsymbol{\beta}}{\partial \mathbf{X}} \ddot{\mathbf{X}} \end{aligned} \tag{25}$$

where:

$$\frac{\partial \boldsymbol{\beta}}{\partial \mathbf{X}} = -\frac{1}{r} \begin{bmatrix} \dfrac{x - A_{1x}}{L_1} & \dfrac{y - A_{1y}}{L_1} \\ \vdots & \vdots \\ \dfrac{x - A_{nx}}{L_n} & \dfrac{y - A_{ny}}{L_n} \end{bmatrix} \tag{26}$$

and $L_i = \sqrt{(x - A_{ix})^2 + (y - A_{iy})^2}$ is the length of cable i, a function of $\mathbf{X} = \{x \quad y\}^T$. By substituting (25) into (22) we obtain:

$$\mathbf{T} = \frac{1}{r}\left(\boldsymbol{\tau} - \mathbf{J}\left(\frac{d}{dt}\left(\frac{\partial \boldsymbol{\beta}}{\partial \mathbf{X}}\right)\dot{\mathbf{X}} + \frac{\partial \boldsymbol{\beta}}{\partial \mathbf{X}} \ddot{\mathbf{X}}\right) - \mathbf{C}\frac{\partial \boldsymbol{\beta}}{\partial \mathbf{X}} \dot{\mathbf{X}}\right) \tag{27}$$

Finally, by combining (19), $\mathbf{ST} = \mathbf{F}_R$, and (27), we obtain the overall dynamics equations of motion, expressed in a standard Cartesian form for robotic systems (Lewis et al., 1993):

$$\mathbf{M}_{eq}(\mathbf{X})\ddot{\mathbf{X}} + \mathbf{N}(\mathbf{X}, \dot{\mathbf{X}}) = \mathbf{S}(\mathbf{X})\boldsymbol{\tau} \tag{28}$$

where the equivalent inertia matrix $\mathbf{M}_{eq}(\mathbf{X})$ and nonlinear terms $\mathbf{N}(\mathbf{X}, \dot{\mathbf{X}})$ are:

$$\mathbf{M}_{eq}(\mathbf{X}) = r\mathbf{m} + \mathbf{S}(\mathbf{X})\mathbf{J}\frac{\partial \boldsymbol{\beta}}{\partial \mathbf{X}} \tag{28a}$$

$$\mathbf{N}(\mathbf{X},\dot{\mathbf{X}}) = \mathbf{S}(\mathbf{X})\left(\mathbf{J}\frac{d}{dt}\left(\frac{\partial \boldsymbol{\beta}}{\partial \mathbf{X}}\right) + \mathbf{C}\frac{\partial \boldsymbol{\beta}}{\partial \mathbf{X}}\right)\dot{\mathbf{X}} \tag{28b}$$

Note the statics Jacobian matrix $\mathbf{S} = \mathbf{S}(\mathbf{X})$ from (23) is a function of Cartesian position $\mathbf{X} = \{x \quad y\}^T$ through the cable angles $\theta_i = \tan^{-1}\left(\frac{y - A_{iy}}{x - A_{ix}}\right)$ (see Figs. 1 and 2).

6. CDDR CONTROLS DEVELOPMENT

This section presents our control architecture and control law development, followed by the dynamic algorithm for calculating actuator torques for CDDRs with two or more degrees of actuation redundancy (this was referred to at the end of Section 4).

6.1 Control Law and Architecture

This sub-section presents our control architecture and control law for translational planar CDDRs based on the overall system Cartesian dynamics equations of motion (28). The input to the plant is the vector of actuator torques $\boldsymbol{\tau}$. Each component of $\boldsymbol{\tau}$ has to be positive or zero at the minimum (in practice, a small positive value). In order to facilitate this problem, let us introduce a virtual generalized Cartesian force input $\mathbf{F}_V$ (units *Nm*):

$$\mathbf{F}_V = \mathbf{S}(\mathbf{X})\boldsymbol{\tau} \tag{29}$$

Since the statics Jacobian matrix **S**(**X**) has dimension 2x*n*, this virtual generalized force input $\mathbf{F}_V$ has the dimension of the translational Cartesian space, 2 in this article. The components of $\mathbf{F}_V$ are not restricted to be positive. If we can develop a control law for the virtual Cartesian force input $\mathbf{F}_V$, it is always possible to find a real controls torque input $\boldsymbol{\tau}$ with all positive components that satisfies (29), if the CDDR position is within the statics workspace. In Section 4.2 we proved that the entire base polygon is within the statics workspace for translational planar CDDRs with regular convex base polygons. Therefore, for control law development, we can consider the new dynamics equation:

$$\mathbf{M}_{eq}(\mathbf{X})\ddot{\mathbf{X}} + \mathbf{N}(\mathbf{X},\dot{\mathbf{X}}) = \mathbf{F}_V \tag{30}$$

We cancel the effects of the nonlinear dynamics terms $\mathbf{N}(\mathbf{X},\dot{\mathbf{X}})$ and account for the inertial terms by using the well-known computed-torque (or feedback linearization) technique (Lewis et al., 1993). We then implement a Cartesian PD controller to reduce the tracking error $\mathbf{e} = \mathbf{X}_R - \mathbf{X}$. The commanded (reference) Cartesian position is $\mathbf{X}_R = \{x_R \quad y_R\}^T$. The computed-torque control law for the virtual Cartesian force input $\mathbf{F}_V$ is:

$$\mathbf{F}_V = \mathbf{M}_{eq}(\mathbf{X}_R)\left(\ddot{\mathbf{X}}_R + \mathbf{K}_P\mathbf{e} + \mathbf{K}_D\dot{\mathbf{e}}\right) + \mathbf{N}(\mathbf{X}_R,\dot{\mathbf{X}}_R) \tag{31}$$

Note we use the reference Cartesian values $\mathbf{X}_R$ in (31). Alternatively, we could use the actual feedback values from actuator encoder sensors and forward pose kinematics. Due to this uncertainty, plus sensor noise problems, plus the problem of digitally twice differentiating the sensor feedback $\mathbf{X}$, we choose $\mathbf{X}_R$ instead.

The control architecture (shown in the block diagram of Fig. 6) is made up of three different parts: the PD controller, the computed-torque terms, and the virtual-Cartesian-force-input-to-real-actuator-torque calculation, with dynamic minimum torque estimation to ensure cable tension is maintained at all times despite the CDDR dynamics. In this article the PD controller gains are determined via pole placement for the resulting effective unit inertia plant, specifying desired settling time and percent overshoot for a unit step input. The matrix gains $\mathbf{K}_P$,$\mathbf{K}_D$ are 2x2 diagonal matrices, which means that the PD control is accomplished independently for the *x* and *y* motions, even though the dynamics model is coupled. We specify the same settling time and percent overshoot for both *x* and *y* motions (see Section 7). The inertial terms $\mathbf{M}_{eq}(\mathbf{X}_R)\ddot{\mathbf{X}}_R$ are composed of the overall position-dependent Cartesian inertia matrix $\mathbf{M}_{eq}$ (28a) and the reference Cartesian acceleration components $\ddot{\mathbf{X}}_R$; the nonlinear terms are $\mathbf{N}(\mathbf{X}_R, \dot{\mathbf{X}}_R)$, given in (28b). The virtual-to-real calculation has the problem to invert the matrix **S**(**X**) that is non-square, such that only positive cable tensions result. This problem is solved in Section 4.2 for CDDRs with one actuation redundancy, and in Section 6.2 below for CDDRs with two or more actuation redundancies.

We do not generally have access directly to Cartesian position **X** feedback via sensors. Instead, we must calculate this feedback using the encoder feedback for each cable pulley angle β_i to determine the cable lengths L_i; these lengths are then used as the inputs to the forward position kinematics solution of Eqs. (3) to calculate Cartesian position **X** for feedback in the control architecture. This feedback scheme will work well only if sufficient tension is maintained on all cables at all times.

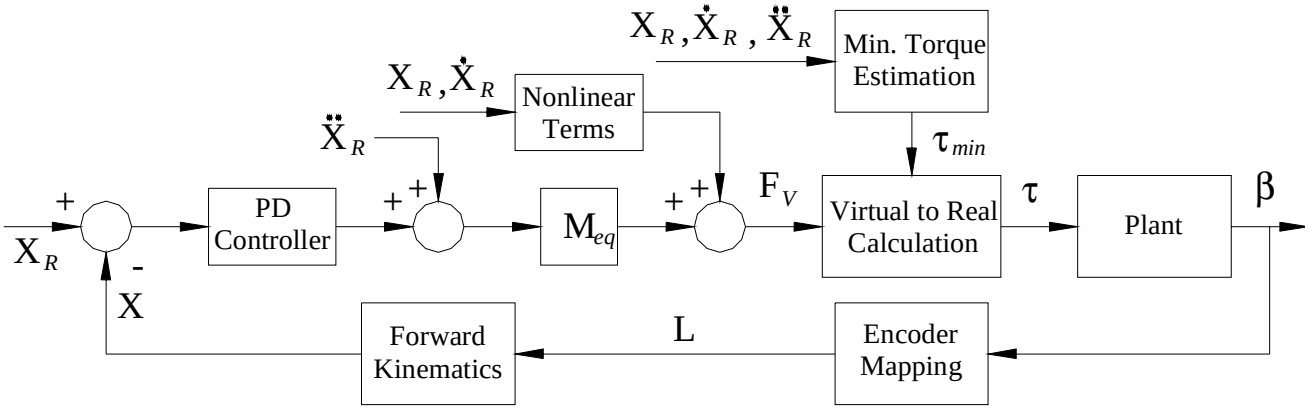

Figure 6. Control Architecture for Translational Planar CDDRs

6.2 Calculation of Optimal Actuator Torques

This sub-section presents a method for determining the optimal actuator torques for the controller architecture of Fig. 6, for CDDRs with two or more degrees of actuation redundancy. This sub-section presents the "Virtual-to-Real Calculation" block of Fig. 6. Also presented is an algorithm for on-line estimation of minimum actuator torques required to maintain positive cable tensions despite the CDDR dynamics; this is the "Minimum Torque Estimation" block in Fig. 6 (which equally applies to CDDRs with one degree of actuation redundancy).

The Jacobian matrix relationship between torques and virtual generalized Cartesian forces is underconstrained in CDDRs, given by (29), $\mathbf{F}_V = \mathbf{S}(\mathbf{X})\boldsymbol{\tau}$. For control we need to calculate the real actuator torques $\boldsymbol{\tau}$ given the virtual forces $\mathbf{F}_V$. For actuation redundancy of degree one, we can adapt the pseudostatics solution of Section 4.2.1 (to this method we must add the dynamic tension estimation algorithm developed below in the current sub-section). For actuation redundancy of degree two or greater, the method is more difficult and is presented in this section, specifically for two actuation redundancies. The solution of the underconstrained system $\mathbf{F}_V = \mathbf{S}(\mathbf{X})\boldsymbol{\tau}$ is similar to (13) from Section 4.2.2, given in (32) for n=4. The difference from (13) is that we can no longer make the pseudostatics assumption $\tau_i = rt_i$ (τ_i is the i^{th} actuator torque, r is the cable pulley radius, and t_i is the i^{th} cable tension). Due to dynamics this assumption no longer holds; we must calculate the required actuator torques for control while attempting to maintain positive cable tensions dynamically.

$$\boldsymbol{\tau} = \begin{Bmatrix} \tau_{P1} \\ \tau_{P2} \\ \tau_{P3} \\ \tau_{P4} \end{Bmatrix} + a \begin{Bmatrix} n_1 \\ n_2 \\ n_3 \\ n_4 \end{Bmatrix} + b \begin{Bmatrix} p_1 \\ p_2 \\ p_3 \\ p_4 \end{Bmatrix} \tag{32}$$

The particular solution $\mathbf{S}^{+}\mathbf{F}_V$ is the first term in (32) and the homogeneous solution is expressed as the two kernel vectors of $\mathbf{S}$ ($\mathbf{N} = \{n_1 \quad n_2 \quad n_3 \quad n_4\}^T$ and $\mathbf{P} = \{p_1 \quad p_2 \quad p_3 \quad p_4\}^T$) multiplied by arbitrary scalars a and b. The goal of torque calculation consists in finding an optimal solution $\boldsymbol{\tau}_{\text{opt}}$ with the following features: 1) Each component of $\boldsymbol{\tau}_{\text{opt}}$, denoted $\{\boldsymbol{\tau}_{\text{opt}}\}_i$, must be greater than or equal to a specified minimum torque $\{\boldsymbol{\tau}_{\min}\}_i$. 2) The norm of $\boldsymbol{\tau}$ must be minimized. The first condition assures that the torque in each motor is always positive, in fact always greater than $\{\boldsymbol{\tau}_{\min}\}_i$. If we don't consider dynamic effects, the tension in each cable turns out to be greater than $r\{\boldsymbol{\tau}_{\min}\}_i$. Under this pseudostatic condition, if $\{\boldsymbol{\tau}_{\min}\}_i$ is set sufficiently high, the cables will never go slack. Unfortunately, when high speed is employed, because of dynamic effects, one or more cable can become slack despite a positive $\{\boldsymbol{\tau}_{\min}\}_i$. In this dynamic case the minimum value for $\{\boldsymbol{\tau}_{\min}\}_i$ must be estimated on-line for each cable in real-time. The on-line cable tension estimation algorithm comes from forcing each tension component to be positive at all times in the dynamics model (27):

$$\{\mathbf{T}\}_i = \left\{ 1/r \left(\tau - \mathbf{J}\left(\frac{d}{dt}\left(\frac{\partial \beta}{\partial \mathbf{X}} \right) \dot{\mathbf{X}} + \frac{\partial \beta}{\partial \mathbf{X}} \ddot{\mathbf{X}} \right) - \mathbf{C} \frac{\partial \beta}{\partial \mathbf{X}} \dot{\mathbf{X}} \right) \right\}_i \geq 0 \qquad i = 1, \cdots, n \qquad (33)$$

The estimated torque solution for each actuator from (33) to maintain cable tension is:

$$\{\boldsymbol{\tau}_{\min}\}_i = \max\left\{ \left\{ \mathbf{J}\left(\frac{d}{dt}\left(\frac{\partial \beta}{\partial \mathbf{X}} \right) \dot{\mathbf{X}} + \frac{\partial \beta}{\partial \mathbf{X}} \ddot{\mathbf{X}} \right) + \mathbf{C} \frac{\partial \beta}{\partial \mathbf{X}} \dot{\mathbf{X}} \right\}_i, 0 \right\} \qquad i = 1, \cdots, n \qquad (34)$$

The reason for the max function in (34) is that when dynamics are taken into account, the minimum torque required to ensure the corresponding cable is in tension could be negative for one or more components. In (34) we force all torque components to be zero at the minimum. For the optimal torque solution, the norm is defined as the simple sum since no components are allowed to be negative:

$$\|\boldsymbol{\tau}(a,b)\| = \sum_{i=1}^{n} \{\boldsymbol{\tau}\}_i \qquad (35)$$

The solution form (32) yields a system of linear non-homogeneous inequalities in the scalar unknowns *a* and *b*.

$$\tau_{Pi} + a\, n_i + b\, m_i \geq \{\boldsymbol{\tau}_{\min}\}_i \qquad i = 1, \cdots, n \qquad (36)$$

Given in this form, we have a typical problem in linear programming, where the objective function (35), the torque norm, must be minimized over a set inequality constraints given by (36). In the solution space $\langle a,b \rangle$, each equation of (36) represents a semiplane whose border is given by the line $\tau_{Pi} + a\, n_i + b\, m_i = \{\boldsymbol{\tau}_{\min}\}_i$, $i = 1, \cdots, n$. When the *n* lines intersect each other, we obtain up to *ni* intersection points (a_l, b_l), $l = 1, \cdots, ni$. We denote this set of points Θ. Note that the maximum number of intersections is $ni = \sum_{j=1}^{n-1} j$. It can be proved (Zionts, 1974) that the optimal $\langle a,b \rangle$ solution is one of these intersections, that is $\boldsymbol{\tau}_{\text{opt}} \in \{\boldsymbol{\tau}(a_l, b_l), l = 1, \cdots, ni\}$. The subset of points of Θ that satisfy the minimum torque requirement (36) is given by:

$$\Theta_{\text{pos}} = \left\{ (a,b) \in \Theta \;\middle|\; \{\boldsymbol{\tau}(a,b)\}_i \geq \{\boldsymbol{\tau}_{\min}\}_i \; \forall\, i = 1, \cdots, n \right\} \qquad (37)$$

We choose the $(a,b) \in \Theta_{\text{pos}}$ that yields the minimum torque norm $N_{\min}$. In conclusion, $\boldsymbol{\tau}_{\text{opt}} = \boldsymbol{\tau}(a_{\text{opt}}, b_{\text{opt}})$, where $(a_{\text{opt}}, b_{\text{opt}})$ belongs to Θ_{pos} and it yields the minimum norm of torques.

Torque Calculation Example for 2 actuation redundancies:

Let us consider the planar 4-cable CDDR (*n*=4) with 2 redundant actuations. Given: virtual generalized Cartesian force $\mathbf{F}_V = \begin{Bmatrix} -1.30 \\ 1.05 \end{Bmatrix}$ (*Nm*), Cartesian position $\mathbf{X} = \begin{Bmatrix} 0.04 \\ -0.23 \end{Bmatrix}$ (*m*), and minimum actuator torques

$\{\boldsymbol{\tau}_{\min}\}_i = 0.10$ (*Nm*), $i = 1,\cdots,4$. From this information, the Jacobian matrix $\mathbf{S(X)}$, the kernel (**N**,**P**) of $\mathbf{S(X)}$, and the particular solution for actuator torques $\boldsymbol{\tau}_P$ are:

$$\mathbf{S(X)} = \begin{bmatrix} -0.97 & 0.95 & 0.46 & -0.56 \\ -0.26 & -0.32 & 0.89 & 0.83 \end{bmatrix} \qquad \begin{Bmatrix} n_1 \\ n_2 \\ n_3 \\ n_4 \end{Bmatrix} = \begin{Bmatrix} -0.74 \\ -0.46 \\ -0.48 \\ 0.11 \end{Bmatrix} \qquad \begin{Bmatrix} p_1 \\ p_2 \\ p_3 \\ p_4 \end{Bmatrix} = \begin{Bmatrix} 0 \\ 0.60 \\ -0.42 \\ 0.68 \end{Bmatrix}$$

$$\begin{Bmatrix} \tau_{P1} \\ \tau_{P2} \\ \tau_{P3} \\ \tau_{P4} \end{Bmatrix} = \begin{Bmatrix} -0.35 \\ -0.69 \\ 0.29 \\ -0.79 \end{Bmatrix}$$

Figure 7 shows the *ni*=6 intersections among the *n*=4 constraint lines. The feasible subspace of the $\langle a,b \rangle$ plane is the upper-left region, as shown in the shaded portion of Fig. 7.

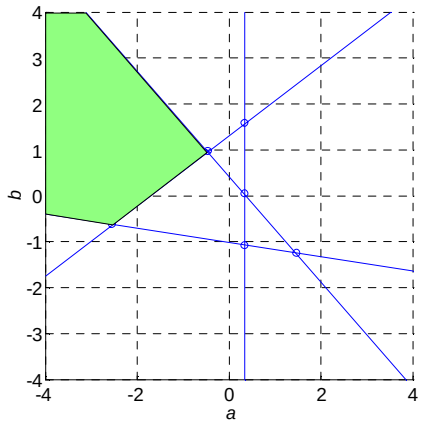

Figure 7. $\langle a,b \rangle$ *Inequality Constraints with Intersections*

The set of the 6 intersection points among the 4 lines is:

$$\Theta = \{(0.34 \quad 1.58), (0.34 \quad 0.06), (0.34 \quad -1.07), (-0.45 \quad 0.97), (-2.54 \quad -0.62), (1.48 \quad -1.25)\}$$

Only two $\langle a,b \rangle$ pairs yield an actuator torque vector $\boldsymbol{\tau}$ with all components greater than $\{\boldsymbol{\tau}_{\min}\}_i$ (only two points border the feasible region in Fig. 7), so the subset of Θ that satisfies (36) is:

$$\Theta_{pos} = \{(-0.45 \quad 0.97), (-2.54 \quad -0.62)\}$$

The member of Θ_{pos} which yields the minimum norm of actuator torques is:

$$(a_{\text{opt}}, b_{\text{opt}}) = \{(-0.45 \quad 0.97)\}$$

and the optimal solutions for actuator torques is:

$$\boldsymbol{\tau}_{\text{opt}} = \{0.69 \quad 0.10 \quad 0.10 \quad 1.40\}^T$$

7. SIMULATION RESULTS

This section presents dynamics and control examples for the translational planar 4-cable CDDR with two degrees of actuation redundancy. These examples demonstrate the CDDR control architecture including feedback linearization and on-line dynamic minimum torque estimation to maintain positive cable tensions despite the dynamics, plus optimal torque calculation for a system with greater than one degree of actuation redundancy. In this section, a given translational planar 4-cable CDDR performs a simulated task twice, the first time without and the second time with the on-line minimum torque estimation algorithm.

The planar 4-cable CDDR model is shown in Fig. 2. The base square has side $L_B = 0.6580$ *m* (this strange number came from our comparison with the 3-cable CDDR in early work; there is no space to show this). The simulated dynamic task is for the CDDR end-effector point $\mathbf{X} = \{x \quad y\}^T$ to trace a circle in the plane. The circle is centered at the base square centroid (the origin of $\{\mathbf{0}\}$) and the circle radius is r = 0.2165 *m* (again, this strange number came from our comparison with the 3-cable CDDR). Figure 8 shows the simulated task to scale for the 4-cable CDDR at the starting (and ending) point. However, to introduce an error for the controller at the start, the end-effector actually starts at 1 *mm* in the positive *Y* direction from the starting point shown in Fig. 8, and it must catch up with the commanded Cartesian motion $\mathbf{X}_R, \dot{\mathbf{X}}_R, \ddot{\mathbf{X}}_R$ and keep the error $\mathbf{e} = \mathbf{X}_R - \mathbf{X}$ small during simulated motion.

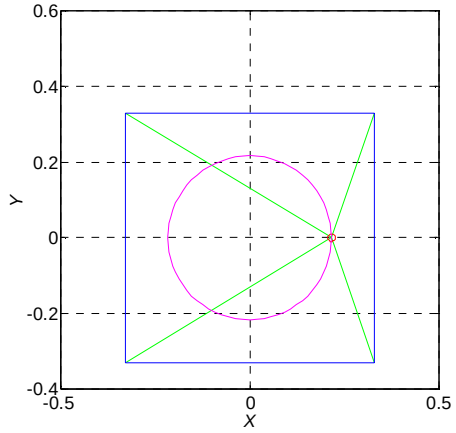

Figure 8. Planar 4-Cable Translational CDDR Example Task

In the simulated example the 4-cable CDDR is commanded to trace the given circle in 1 *sec* (zero Cartesian force $\mathbf{F}_R$ is specified). We define polar angle ϕ as the independent parameter for the circle; it is measured using the right-hand from the right horizontal to the circle radius; ϕ is shown at 0 (and 360°) in Fig. 8. We provide a constant acceleration for the first half of the circle and an equal constant deceleration for the second half of the circle; the commanded motion starts and ends at zero velocity. The kinematic task

relationships for this desired reference motion are $\alpha = \dot{\omega} = \ddot{\phi} = 8\pi$, $\omega = \dot{\phi} = \alpha t$, and $\phi = \alpha t^2 / 2$ for the first half of the circle; the second half is symmetric to the first. The associated commanded (reference) Cartesian position $\mathbf{X}_R$, velocity $\dot{\mathbf{X}}_R$, and acceleration $\ddot{\mathbf{X}}_R$ for use in the controller architecture are easy to determine.

The parameters for the dynamics equations of motion (28) for the 4-cable CDDR are: point mass *m* = 1 *kg*; rotational shaft/pulley inertias $J_i = 0.0008$ kgm^2 (for all $i = 1, \cdots, 4$); shaft rotational viscous damping coefficients $c_i = 0.01$ *Nms* (for all $i = 1, \cdots, 4$); and $r_i = r = 5$ *cm* (for all $i = 1, \cdots, 4$).

The Cartesian PD controller is found by standard pole placement techniques (the feedback linearization approach makes the plant appear linear, as a unit inertia), specifying a 0.2 *sec* settling time and 5% percent overshoot. We design for Cartesian *x* and *y* directions independently, with the same settling time and percent overshoot specifications. Gain $\mathbf{K}_P$ is a 2x2 diagonal matrix with equal gains of $K_P = 839.9$ on the diagonal, and gain $\mathbf{K}_D$ is a 2x2 diagonal matrix with equal gains of $K_D = 40$ on the diagonal.

A Matlab *Simulink* simulation based on Fig. 6 and the methods of this article was developed to produce the results given in this section. Two control simulations of the dynamics model are presented in this section for the 4-cable CDDR, both without and with the on-line minimum torque estimation algorithm of Fig. 6.

Figures 9a-c show the minimum actuator torques, actual actuator torques, virtual generalized Cartesian forces, and actual cable tensions, respectively, for the circle task, *without* the on-line minimum torque estimation algorithm.

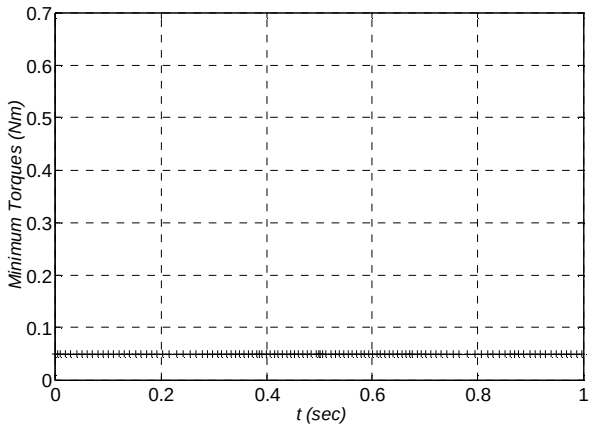

Figure 9a. Minimum Actuator Torques
τ_1 (solid), τ_2 (long dash), τ_3 (short dash), τ_4 (*)

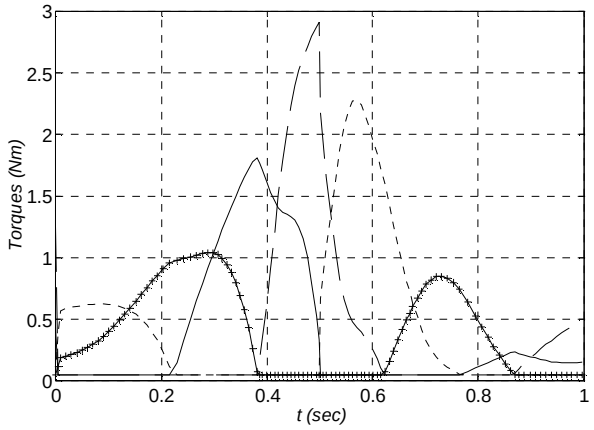

Figure 9b. Actual Actuator Torques
τ_1 (solid), τ_2 (long dash), τ_3 (short dash), τ_4 (*)

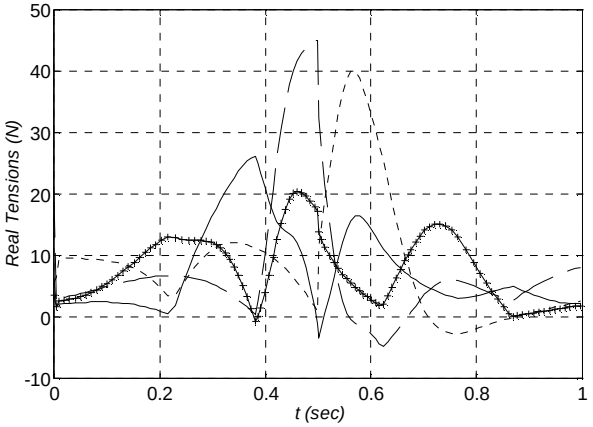

Figure 9c. Actual Cable Tensions
t_1 (solid), t_2 (long dash), t_3 (short dash), t_4 (*)

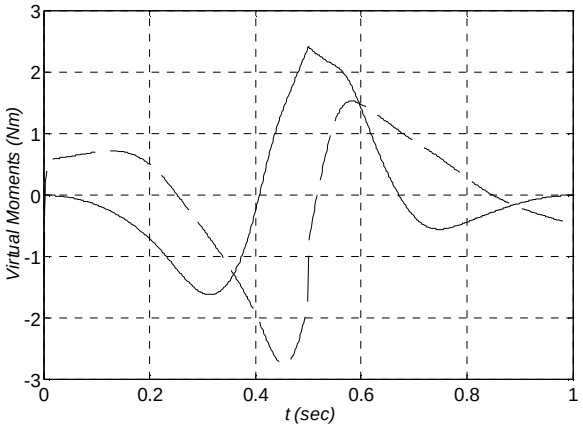

Figure 10. Virtual Generalized Cartesian Forces (Nm)
F_{Vx} (solid) *and* F_{Vy} (dash)

As shown in Fig. 9a, for the simulation *without* the on-line minimum torque estimation algorithm, the minimum torques are constant and identical for all actuators, taking a specified value of 0.05 *Nm* in this example. The control torques, calculated by the optimal method in the Virtual to Real Calculation block of Fig. 6, but without the Min. Torque Estimation block, are shown in Fig. 9b. Actuator torques 1, 2, and 3 peak near the center of motion time, due to the maximum velocity occurring at this point; torque 4 peaks twice, nearer the start and end of motion. During motion all four torques at different times yield negative values in the Virtual to Real Calculation, but these are limited to a small positive value, the constant specified minimum torque of 0.05 *Nm*. The associated actual cable tensions resulting from the simulated motion considering the dynamics model are shown in Fig. 9c. For this simulated motion, the *x* and *y* components of the virtual generalized Cartesian forces are shown in Fig. 10; these are not limited to be positive. Without including the dynamic minimum tension estimation algorithm, each cable tension becomes negative and thus slack at different times during the simulated motion. Clearly this is unacceptable as control would be lost in these ranges of motion. Thus, the constant minimum tension specification is suitable only for pseudostatic motions, not for dynamic motions with high velocities and accelerations.

Figures 11a-c show the minimum actuator torques, actual actuator torques, and actual cable tensions, respectively, for the same circle task, *with* the on-line minimum torque estimation algorithm. As shown in Fig. 11a, for the simulation *with* the on-line minimum torque estimation algorithm, the minimum torques are no longer constant, but vary (greater than the minimum positive torque) so that no cable tensions will go negative in the dynamics model. The control torques, obtained by including the Min. Torque Estimation block in the Virtual to Real Calculation, are shown in Fig. 11b. Again, during motion all four torques yield negative values but these are limited to the minimum torque of 0.05 *Nm* in these ranges. Though Figs. 9a and 11a are quite different (minimum torques *without* and *with* the dynamic minimum torque estimation), the resulting control torques of Figs. 9b and 11b are similar, though not identical. The simulated cable tensions considering the dynamics model are shown in

Fig. 11c. By including the dynamic minimum torque estimation algorithm, each cable tension never becomes negative and thus control is maintained at all times. In Fig. 11c we allow zero cable tension as a minimum; in practice a small positive value should be used instead. Figs. 9c and 11c are very similar in shape and magnitude; however, Fig. 11c is a big improvement over Fig. 9c, where all cables were negative for a portion of the motion. Thus, we must include the dynamic minimum torque estimation algorithm for challenging dynamic motions.

The virtual generalized Cartesian forces are not shown for this case because they are identical to those of Fig. 10; for the identical Cartesian circle task, $\mathbf{F}_V$ will be identical regardless of including or not including the algorithm for estimating minimum actuator torques.

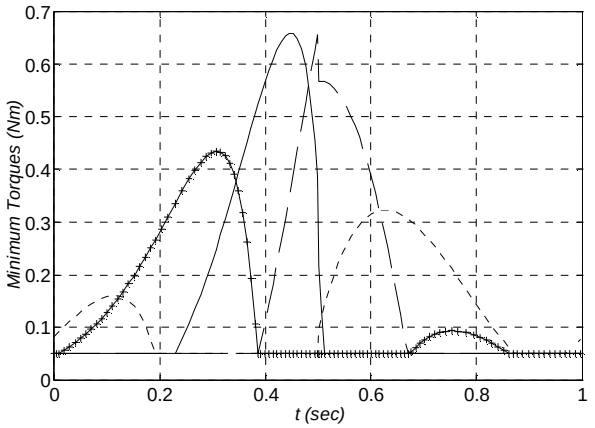

Figure 11a. Minimum Actuator Torques
τ_1 (solid), τ_2 (long dash), τ_3 (short dash), τ_4 (*)

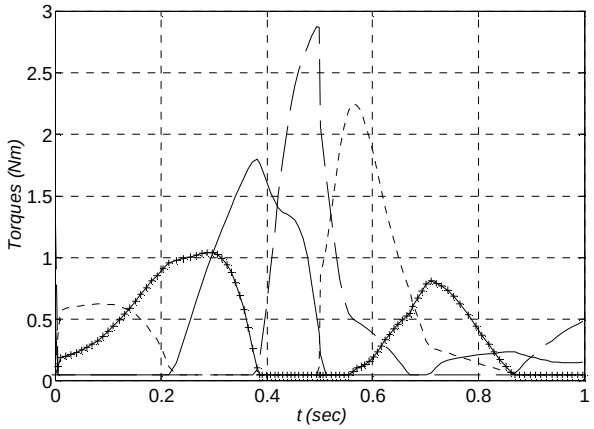

Figure 11b. Actual Actuator Torques
τ_1 (solid), τ_2 (long dash), τ_3 (short dash), τ_4 (*)

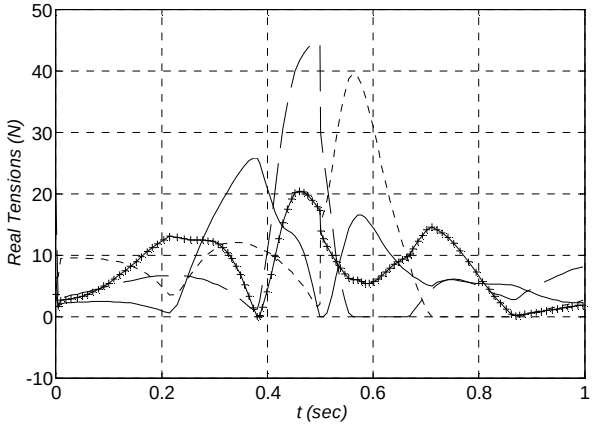

Figure 11c. Actual Cable Tensions
t_1 (solid), t_2 (long dash), t_3 (short dash), t_4 (*)

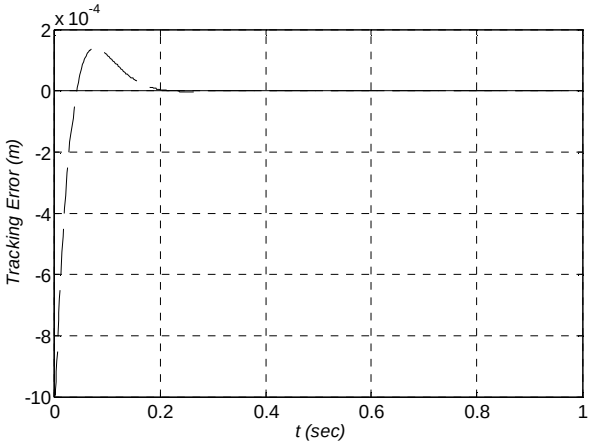

Figure 12. Simulated Tracking Error

For the latter control case, including the dynamic minimum torque estimation algorithm, the simulated controller tracking error is shown in Fig. 12. This plot shows the Euclidean norm of the tracking error,

$\sqrt{(x_R - x)^2 + (y_R - y)^2}$. The simulation starts with an artificial error of 1 *mm* in the *Y* direction to demonstrate the error convergence. In the former control case, *without* the dynamic minimum torque estimation algorithm, where one (or more) cable loses tension, the tracking error is much worse than Fig. 12 since all cable go slack at different times in the simulation, causing a large Cartesian error (not shown). The control architecture will work well only if all cables are under tension at all times; therefore, the dynamic minimum torque estimation algorithm must be used.

8. CONCLUSION

This article introduces translational planar cable-direct-driven robots (CDDRs). The motivation behind this work is to answer the serious cable interference and negative cable tensions possible with existing CDDRs that provide both translational and rotational motions. Of course, a big disadvantage of translational CDDRs is that they may only be used for a subset of planar tasks, where no rotations or moment resistance is required at the end-effector. Kinematics and statics modeling is presented, followed by determination of the statics workspace (the space wherein all possible Cartesian forces may be exerted with only positive cable tensions). Dynamics modeling and controls development with feedback linearization for translational planar CDDRs with one- or two- (and higher) degrees of actuation redundancy was presented. The control architecture will work well only if sufficient tension is maintained on all cables at all times. Simulations were given to compare the 4-cable CDDR in the same task, without and with the novel dynamic minimum torque estimation algorithm.

It was found that the dynamic minimum torque estimation algorithm was required for CDDR motions with high velocities and accelerations. Otherwise, the simulation revealed that each of the cables becomes slack during motion and thus control is lost. The computed-torque, or feedback linearization technique performed perfectly in simulation, i.e. when we assume we know the dynamic model perfectly, the inertial effects and nonlinear dynamics terms are cancelled perfectly. Therefore, in the future we will focus on implementing robust control techniques to preserve good error tracking despite modeling uncertainties. Our future work plans also include dynamic stiffness modeling, more complete dynamics modeling (cable inertia and stiffness, Coulomb friction, among others), hardware implementation, and experimental validation of our results.

REFERENCES

1. J.S. Albus, R. Bostelman, and N.G. Dagalakis, 1993, "*The NIST ROBOCRANE*", Journal of Robotic Systems, 10(5): 709-724.

2. G. Barette and C.M. Gosselin, 2000, "*Kinematic Analysis and Design of Planar Parallel Mechanisms Actuated with Cables*", ASME Design Technical Conferences, Baltimore, MD.

3. P.D. Campbell, P.L. Swaim, and C.J. Thompson, 1995, "*Charlotte Robot Technology for Space and Terrestrial Applications*", 25th International Conference on Environmental Systems, San Diego, SAE Article 951520.

4. W. Choe, H. Kino, K. Katsuta, and S. Kawamura, 1996, *"A Design of Parallel Wire-Driven Robots for Ultrahigh Speed Motion Based on Stiffness Analysis"*, ASME Japan/USA Symposium on Flexible Automation, 1:159-166.

5. C.M. Gosselin, 1996, "Parallel Computation Algorithms for the Kinematics and Dynamics of Planar and Spatial Parallel Manipulators", *Journal of Dynamic Systems, Measurement, and Control*, 118(1): 22-28.

6. S. Kawamura and K. Ito, 1993, *"New Type of Master Robot for Teleoperation Using a Radial Wire Drive System"*, Proceedings of the IEEE/RSJ International Conference on Intelligent Robots and Systems, Yokohama, Japan, July 26-30, 55-60.

7. S. Kock and W. Schumacher, 2000, *"Control of Fast Parallel Robot with a redundant Chain and Gearboxes: Experimental Results"*, IEEE International Conference on Robotics and Automation: 1924-1929.

8. F.L. Lewis, C.T. Abdallah, and D.M. Dawson, 1993, Control of Robot Manipulators, MacMillan, New York.

9. R. Lindemann and D. Tesar, 1989, "*Construction and Demonstration of a 9-String 6-DOF Force Reflecting Joystick for Telerobotics*", NASA International Conference on Space Telerobotics, (4): 55-63.

10. R.G. Roberts, T. Graham, and T. Lippitt, 1998, "*On the Inverse Kinematics, Statics, and Fault Tolerance of Cable-Suspended Robots*", Journal of Robotic Systems, 15(10): 581-597.

11. Y. Shen, H. Osumi, and T. Arai, 1994, *"Manipulability Measures for Multi-wire Driven Parallel Mechanisms"*, IEEE International Conference on Industrial Technology, 550-554.

12. L.W. Tsai, 1999, Robot Analysis: The Mechanics of Serial and Parallel Manipulators, Wiley, New York.

13. S. Walairacht, Y. Koike, and M. Sato, *"A new haptic display for both-hands-operation: SPIDAR-8"*, 1999 IEEE International Symposium on Intelligent Signal Processing and Communication Systems: 569-72.

14. R.L. Williams II, 1998, *"Cable-Suspended Haptic Interface"*, International Journal of Virtual Reality, 3(3): 13-21.

15. R.L. Williams II and P. Gallina, 2002, "*Planar Cable-Direct-Driven Robots: Design for Wrench Exertion*", Journal of Intelligent and Robotic Systems, 35(2): 203-219.

16. S. Zionts, 1974, Linear and Integer Programming, Englewood Cliffs, N.J., Prentice-Hall.